DE GRUYTER OPEN

Nova Biotechnol Chim (2017) 16(2): 138-146
DOI: 10.1515/nbec-2017-0019

Nova Biotechnologica *et* Chimica

Diamagnetic cobalt(III)tris(o-ethylxanthate) and nickel(II)bis(o-ethylxanthate)

Filip Varga[1], Ján Titiš[1], Cyril Rajnák[1,✉], Ján Moncoľ[2] and Roman Boča[1]

[1] *Department of Chemistry, Faculty of Natural Sciences, University of SS. Cyril and Methodius in Trnva, Nám. J. Herdu 2, Trnava, SK-917 01, Slovak Republic*

[2] *Institute of Inorganic Chemistry, FCHPT, Slovak University of Technology, Bratislava, SK-812 37, Slovak Republic*

Article info

Article history:
Received: 11th October 2017
Accepted: 16th November 2017

Keywords:
Ab initio calculations
Co(III) complex
Magnetism
Ni(II) complex
O-ethyl xanthate
UV-VIS spectra

Abstract

Diamagnetic [Co(*xanth*)$_3$] and [Ni(*xanth*)$_2$] complexes have been prepared by reaction of Co(II) and Ni(II) salts with potassium *O*-ethyl xanthate (K*xanth*). The isolated Co(III) and Ni(II) complexes have been characterized by single-crystal X-ray crystallography, UV-VIS and IR spectroscopy, computational methods, and magnetic measurements.

Introduction

Transition metal complexes containing chelating ligands are the subjects of extensive research for a long time due to the broad range of their structural, spectral and magnetic properties (Gerloch and Constable 1994). In the past few decades, such coordination compounds have attracted increased attention of chemists because of their potential applications in various fields as chemical sensors, nonlinear optical materials and/or molecular magnetic materials (Noro *et al.* 2009).

Over the past ten years, an extraordinary interest on single-molecule magnets (SMMs) has been registered. Single-molecule magnets, attractive for high-density information storage and quantum computing, are metal complexes, that beside other interesting quantum phenomena, exhibit slow relaxation of the magnetization. The earlier type of SMMs was based on high-spin polynuclear complexes, such as a dodecanuclear plaquette-type complex known as Mn12ac. In course of time a plethora 3d-metal complexes were identified as SMMs, including simple mononuclear systems containing Mn(III) (Grigoropoulos *et al.* 2013), Fe(III) (Mossin *et al.* 2012), Fe(II) (Feng *et al.* 2013), Fe(I) (Samuel *et al.* 2014), Co(II) (Rajnák *et al.* 2017), Ni(II) (Lomjansky *et al.* 2017), Ni(I) (Lin *et al.* 2016) and Cu(II) (Boča *et al.* 2017) central atoms (Frost *et al.* 2016). Among these systems, the S-donor ligands combined with the cobalt(II) centres attract a considerable attention because of the pronounced magnetic anisotropy that supports the SMM behaviour (Zadrozny and Long 2011). However, Co(II) can be readily oxidized to Co(III) in course of the complexation reaction on air giving rise the diamagnetic complex. Tetracoordinate Ni(II) complexes in their nearly tetrahedral geometry are also promising SMMs. Some ligands prefer the square planar arrangement around the Ni(II) central atom and these complexes are diamagnetic as well. Some relationships between the structure and magnetic properties are compared in Table 1. Herein we are

✉ *Corresponding author:* cyril.rajnak@ucm.sk

Table 1. Comparison of structure-magnetism relationships for related compounds.

Complex	Chromophore	Magnetic property	Reference
$(Ph_4P)_2[Co(SPh)_4]$	Tetrahedral	SMM	Zadrozny and Long 2011
$[Co(PPh_3)_2Cl_2]$	Tetrahedral	SMM	Yang *et al*. 2013
$[Co(PPh_3)_2Br_2]$	Tetrahedral	SMM	Boča *et al*. 2014
$[Co(PPh_3)_2I_2]$	Tetrahedral	SMM	Saber and Dunbar 2014
$[Co(PPh_3)_2(SCN)_2]$	Tetrahedral	SMM	Rajnák *et al*. 2016
$[Ni(PPh_3)_2Cl_2]$	Tetrahedral	Paramagnet, no SMM	Lomjanský *et al*. 2016
$[Ni(PPh_3)_2(NCS)_2]$	Planar	Diamagnet, no SMM	Rajnák, unpublished

reporting about synthesis, characterization and structural properties of the [Co(*xanth*)$_3$] and [Ni(*xanth*)$_2$] complexes with chelating S-donor ligand which were found to be diamagnetic.

Experimental

Chemicals and handling

All inorganic and organic reactants of reagent grade quality were purchased and used as received (Sigma-Aldrich). The solvents ethanol and acetonitrile were used without further purification.

Synthesis of [Co(*xanth*)$_3$] (**1**)

The compound **1** has been prepared as follows. 0.16 g (1 mmol) of potassium *O*-ethyl xanthate, was dissolved in ethanol (10 cm^3) under an intense stirring. 0.064 g of cobalt(II) chloride was also dissolved in 10 cm^3 of ethanol under an intense stirring (the molar ratio of *xanth*: cobalt(II) chloride = 2:1). The two solutions were mixed and the final solution was refluxed for 4 hours. The filtrate was left for the duration of 5 days for a spontaneous evaporation. Deep dark green crystals were obtained by slow evaporation of the solution at room temperature. Yield: 0.085 g Anal. Calc. for 1, $C_9H_{15}CoO_3S_6$ (M = 422.57 g mol^{-1}): C, 25.58; H, 3.58; S, 45.53. Found: C, 25.88; H, 3.56; S, 46.02. Selected IR bands (KBr) ν/cm^{-1}: 2976(w), 2484(w), 1898(w), 1861(w), 1721(w), 1464(w), 1444(m), 1433(m), 1387(m), 1365(s), 1273(w), 1233(s), 1143(w), 1116(s), 1055(w), 1030(s), 1000(s), 861(m), 810(w), 657(w), 548(w), 438(s). UV/Vis (Nujol) $\nu_{max}/10^3$ cm^{-1} (relat. absorb.): 15.8 (0.435), 20.7 (0.526).

Synthesis of [Ni(*xanth*)$_2$] (**2**)

The compound **2** was prepared as follows. A 100 cm^3 round bottom flask was charged with potassium ethyl xanthogenate (0.150 g, 0.94 mmol) and acetonitrile (20 cm^3) and slight heated. $NiCl_2 \cdot 6H_2O$ (0.111 g, 0.47 mmol) was added once. Yellowish solution changed colour immediately to green. Reaction was heated with an oil bath for four hours at 80°C. In process of cooling a mixture changed colour to brown. After 3 days dark red crystalline compound was filtered off and dried in vacuum. Yield: 0.026 g. Anal. Calc. for 1, $C_6H_{10}NiO_2S_4$ (M = 301.10 g mol^{-1}): C, 23.93; H, 3.35; S, 42.60. Found: C, 24.14; H, 3.05; S, 41.13. Selected IR bands (KBr) ν/cm^{-1}: 2982(w), 2935(w), 2891(w), 2503(w), 1464(m), 1429(w), 1388(w), 1366(s), 1325(w), 1244(s), 1144(w), 1113(s), 1058(w), 1020(s), 996(s), 855(m), 808(w), 662(w), 554(w), 435(s) (s – strong, m – medium, w-weak); S-C=S (554 cm^{-1}), C=S (1058 – 1144 cm^{-1}), C-O-C (855 cm^{-1}), νCH3 (2935 cm^{-1}), νCH2 (2891 cm^{-1}) a δC-H (1325 – 1464 cm^{-1}). UV/Vis (Nujol) $\nu_{max}/10^3$ cm^{-1} (relat. absorb.): ~15.0 (0.191), 20.7 (0.459), 23.8 (0.513).

Physical measurements

Elemental analyses were carried out by Flash 2000 CHNS apparatus (Thermo Scientific). The IR spectra were measured on ATR holder with highly effective diamond crystal in the region of 4000 – 400 cm^{-1} by Nicolet 5700 spectrometer (Thermo Electron) with DTGS/KBr detector. The solid sample for FT-IR measurements was not dried prior to its using and was used as freshly synthesized. Absorption UV-Vis spectra for solid sample (Nujol mull) were measured by Specord.

Table 2. Crystal data and structure refinement for **1**, **2**.

Empirical formula	$C_9H_{15}CoO_3S_6$	$C_6H_{10}NiO_2S_4$
Formula weight (g.mol^{-1})	422.50	301.09
Crystal system	trigonal	orthorhombic
Space group	*R*–3	*P*bca
T (K)	100(1)	100(1)
a (Å)	14.8164(14)	7.4174(8)
b (Å)	14.8164(14)	7.1003(6)
c (Å)	12.8790(12)	20.760(2)
α (°)	90	90
β (°)	90	90
γ (°)	120	90
V (Å^3)	2 448.5(5)	1 093.36(19)
ρ_{calc} (g.cm^{-3})	1.719	1.829
Z	6	4
Radiation type	Cu Kα	Cu Kα
μ (mm^{-1})	1.54186	1.54186
F(000)	1 296	616
Abs. coefficient	15.426	9.439
R_1[F2 > 2σ(F2)], wR_2(F2)	0.0328, 0.0755	0.0476, 0.1220
$\Delta\rho_{max}$, $\Delta\rho_{min}$ (e Å^{-3})	0.45, -0.59	1.45, -0.45
CCDC no.	1569076	1569077

250 Plus (Analytica Jena) with the DAD detector in the range of 9 000 – 50 000 cm^{-1}. Magnetic data was taken with the SQUID apparatus (Quantum Design, MPMS-XL7) in the RSO mode of the detection. The detected magnetic moment of the specimen has been converted to the molar magnetic susceptibility χ_{mol} and the dimensionless product function $\chi T/C_0$ with the reduced Curie constant $C_0 = N_A\mu_0\mu_B^2/k_B$ containing the fundamental physical constants in their usual meaning.

X-ray crystal structure determination

Data collection and cell refinement of **1**, **2** were made by Stoe StadiVari diffractometer using PILATUS3R 300K HPAD detector and micro-focused source Xenocs FOX3D with CuKα at 100K. Corrections to Lorentz, polarization and multi-scan absorption effects were applied. The structure was solved by charge-flipping or direct methods and refined anisotropically by common least-squares methods. The programs SUPERFLIP (Palatinus and Chapuis 2007), SHELXT (Sheldrick 2015), SHELXL (ver. 2016/6) (Sheldrick 2015) and OLEX2 (Dolomanov *et al.* 2009) have been used for structure determination, refinement and drawing. The hydrogen atoms were refined with fixed distances from the parent carbon atoms. Crystal data on **1**, **2** are presented in Table 2.

Results and Discussion

Structural data

The compound **1**, [Co(*xanth*)$_3$], possesses a molecular structure. The central Co(III) atom is hexacoordinate by three bidentate *xanth* ligands (Fig. 1). The Co-S distances are almost identical (2.268 – 2.282 Å, see Table 3). As expected, the S-Co-S angles are acute (41 – 51 deg). The compound **1**, [Co(*xanth*)$_3$], crystallizes in trigonal system in space group *R*–3. The cobalt atom lies on 3-fold axis and is coordinated in distorted octahedron. The coordination octahedron around cobalt atom of **1** is formed by six sulfur atoms [Co1–S1 = 2.2693(7) Å and Co1–S2 = 2.2743(8) Å (Table 3)] of three bidentate carbamate group of *xanth*.

The compound **2**, [Ni(*xanth*)$_2$] crystallize in orthorhombic system in space group *P*bca (Table 2) and it possesses a molecular structure with the planar chromophore {Ni^{II}S$_4$} – see Fig. 2. The nickel atom lies in the centre of symmetry and is bonded by four sulfur atoms [Ni1–S distance in region 2.21– 2.22 Å (Table 4)] of two bidentate carbamate groups of *xanth* square-planar coordination.

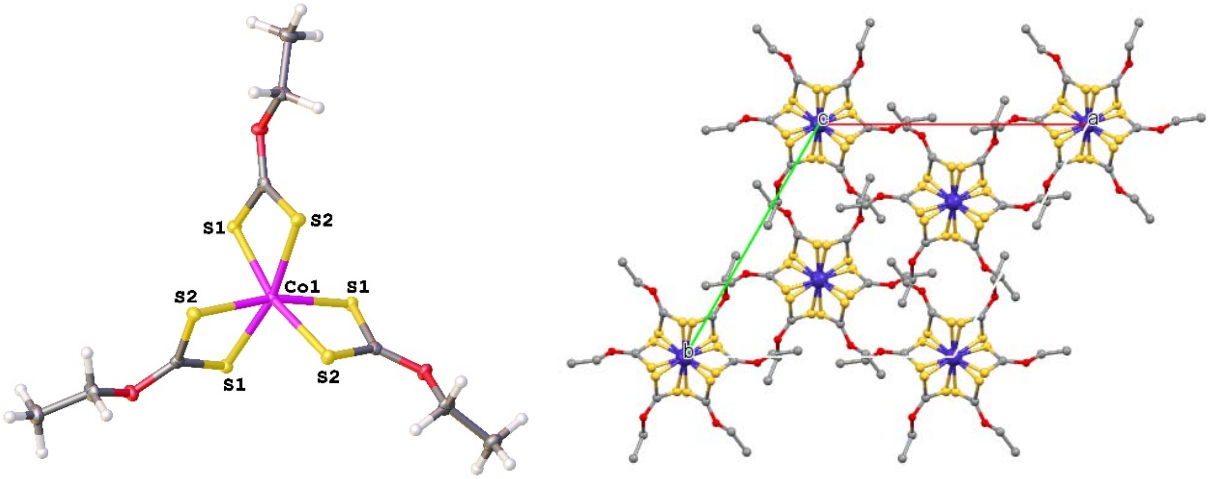

Fig. 1. Molecular and crystal structure of complex [Co(*xanth*)$_3$], **1**.

Table 3. Selected bond lengths (Å) and angles (°) in complex **1**.

Co1–S1	2.2693(7)	Co1–S2	2.2743(8)
Co1–S1^{i}	2.2693(7)	Co1–S2^{i}	2.2743(8)
Co1–S1^{ii}	2.2693(7)	Co1–S2^{ii}	2.2744(8)
S1–Co1–S1^{i}	94.18(3)	S1–Co1–S1^{ii}	94.19(3)
S1^{i}–Co1–S1^{ii}	94.19(3)	S1^{ii}–Co1–S2^{i}	166.63(2)
S1–Co1–S2	76.73(2)	S1^{i}–Co1–S2	166.63(2)
S1–Co1–S2^{ii}	166.63(2)	S1^{i}–Co1–S2^{ii}	96.22(2)
S1^{i}–Co1–S2^{i}	76.73(2)	S1–Co1–S2^{i}	96.22(2)
S1^{ii}–Co1–S2^{ii}	76.73(2)	S1^{ii}–Co1–S2	96.22(2)
S2^{i}–Co1–S2	94.31(3)	S2^{i}–Co1–S2^{ii}	94.31(3)
S2–Co1–S2^{ii}	94.31(3)		

Symmetry codes: (i) 1-*y*, *x*-*y*, *z*; (ii) 1+*y*-*x*, 1-*x*, *z*

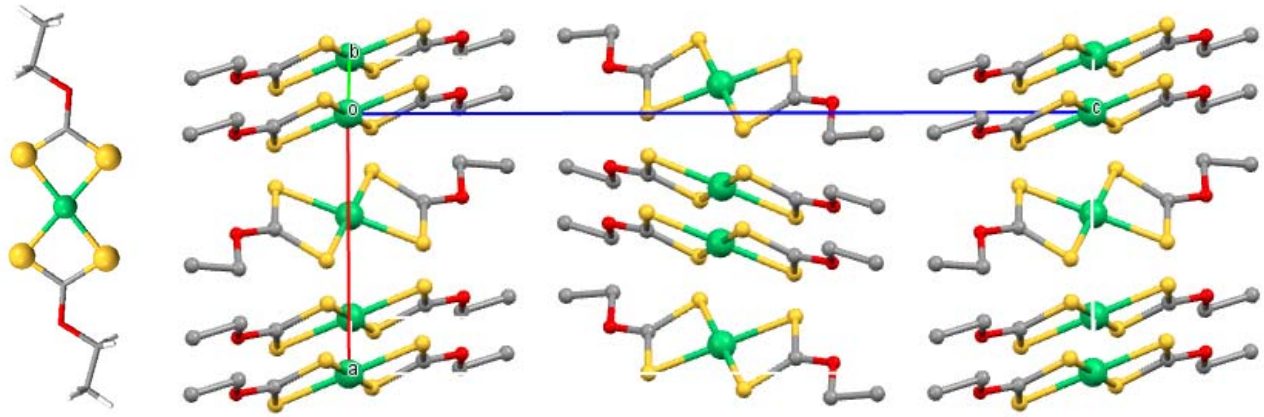

Fig. 2. Molecular and crystal structure of the complex [Ni(*xanth*)$_2$], **2**.

Electronic spectra

The solid state electronic spectra of **1** and **2** measured in Nujol mull are presented in Fig. 3. These complexes exhibit a similar spectral profile with a number of electronic transitions that have varying peak intensity. The first visible transitions are slightly intense and located in the range of 15 000 – 25 000 cm^{-1}. This part of the spectrum is almost identical for both complexes. In this range

we can identify two transitions at ~15 000 and 20 000 cm^{-1}. Moreover, in the spectrum of the Ni(II) complex another peak is visible at ~24 000 cm^{-1}. For the Co(III) complex this transition is missing, however, there is a broad asymmetric band in this location with a maximum at 28 000 cm^{-1}. More intense and clearly identifiable peaks are located in the range of 30 000 – 50 000 cm^{-1}.

Table 4. Selected bond lengths (Å) and angles (°) in complex **2**.

Ni1–S1	2.2182(8)
Ni1–S1^{iii}	2.2183(8)
Ni1–S2	2.2201(7)
Ni1–S2^{iii}	2.2201(7)
S1–Ni1–S1^{iii}	180.0
S1–Ni1–S2	79.43(3)
S1^{iii}–Ni1–S2^{iii}	79.43(3)
S1^{iii}–Ni1–S2	100.57(3)
S1–Ni1–S2^{iii}	100.57(3)
S2–Ni1–S2^{iii}	180.0

Symmetry codes: (iii) 1-*x*, -*y*, 1-*z*; (iv) -*x*, 1-*y*, -*z*

The hexacoordinate Co(III) complexes in the strong crystal field possess the electronic ground term $^1A_{1g}$ that is well separated from its excited counterparts. A modelling using the generalized crystal-field theory (GCFT) with the crystal field poles F_4 = 20 000 cm^{-1} ($10Dq$ = 33 333 cm^{-1}) lifts the first spin-allowed d-d transition to E_1 = 26 000 cm^{-1} ($^1A_{1g}$ → $^1T_{1g}$) and the second one to E_2 = 28 000 cm^{-1} ($^1A_{1g}$ → $^1T_{2g}$). The square-planar Ni(II) complexes in the strong crystal field also possess the electronic ground term $^1A_{1g}$. A modelling by the GCFT with the crystal field poles F_2 = 20 000 and F_4 = 10 000 cm^{-1} gave the lowest spin-allowed excitation energies at E_1 = 14 900 cm^{-1} ($^1A_{1g}$ → $^1A_{2g}$) and E_2 = 21 300 cm^{-1} ($^1A_{1g}$ → $^1B_{1g}$). *Ab initio* calculations based on multireference CASSCF method improved by NEVPT2 approach have been performed to verify the crystal-field. theory results. To this end, the active space extended by the second d-shell (*n* electrons, where *n* = 6 for Co(III) and 8 for Ni(II), were correlated in 10 orbitals) and def2-TZVP basis set were used within these calculations. Averaging of 10 triplet and 15 singlet states of Ni(II) and 5 quintet, 45 triplet and 50 singlet states of Co(III) was utilized. The results obtained for the experimental geometry of complexes are collected in Table 5. It can be seen, the agreement between the GCFT and *ab initio* results is good (Table 6). Thus, estimation of the crystal field poles in the previous analysis and the conclusions that follow may be considered correct. Comparison of the calculated results with the experimental spectra also confirms this claim.

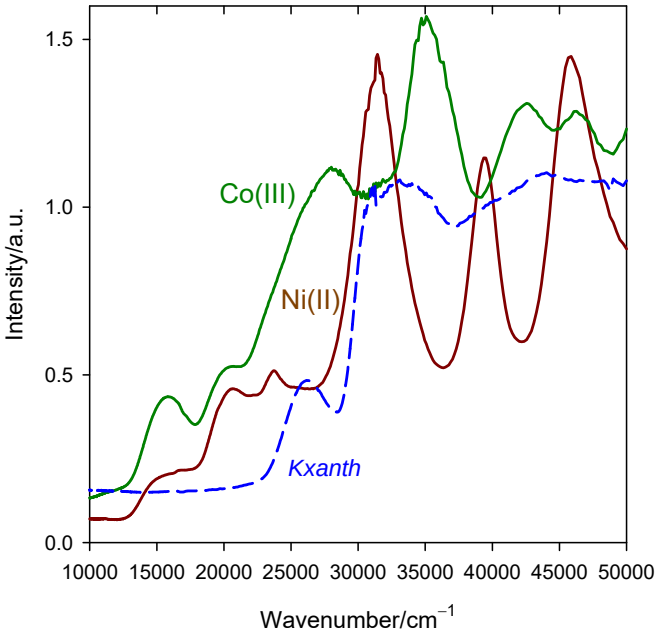

Fig. 3. Solid state electronic spectra for complexes **1** and **2**. Spectrum of the K*xanth* is added for comparison.

Table 5. Assignment of transitions in **1** and **2**.

1		**2**	
experimental	***ab initio***	**experimental**	***ab initio***
11000 w	13500 $^3T_{1g}$		2800 – 4300
16000 m	18100 $^5T_{2g}$	13500 sh	13500 ^3E_g
20500 m	19400 $^3T_{2g}$	16000 m	16700, 17800,
28000 s	21500 $^1T_{1g}$	20600 m	18200
31500 s	32800 $^1T_{2g}$	23700 m	23400 $^3B_{2g}$, 23400
35000 s	34400 $^3T_{2g}$	31500 s	
36500 s	36500 $^3T_{1g}$	39500 s	36000

w – weak, m – medium, s – strong, sh – shoulder

Table 6. Calculated transition energies below 50 000 cm^{-1} for **1** and **2**[a].

1, [Co(*xanth*)$_3$]				**2**, [Ni(*xanth*)$_2$]			
GCFT		CASSCF-NEVPT2		GCFT		CASSCF-NEVPT2	
Term	Energy	Mult.	Energy	Term	Energy	Mult.	Energy
$^1A_{1g}$	0	1	0	$^1A_{1g}$	0	1	0
$^5T_{2g}$	15095 15095	3	13433	$^3B_{1g}$	4179	3	2770
	15095 16003	3	13471	$^3A_{2g}$	4554	3	2967
	16003 16003	3	13487	^3E_g	7588	3	4288
$^3T_{1g}$	16045 16045	5	18097		7588	3	13502
	16045 26046	5	18126	$^1A_{2g}$	14900	1	16677
	26046 26046	5	18158	$^3B_{2g}$	20846	1	17813
$^3T_{2g}$	28160 28160	3	19305	$^1B_{1g}$	21277	1	18257
	28160 39708	3	19454	^1E_g	23443	3	23399
	39708 39708	3	19461		23443	1	23438
$^1T_{1g}$	39738 39738	1	21442	^3E_g	23970	3	24332
	39738 43430	1	21459		23970	3	25556
	43430 45803	1	21479	$^1A_{1g}$	31317	3	26762
$^1T_{2g}$	45803 45803	1	32393	$^1B_{2g}$	37520	3	36081
	46315 46315	1	32891	$^3A_{2g}$	38958	1	37096
	46315 48429	1	32907	^1E_g	41225	3	37965
$^3T_{2g}$	48429	3	34281		41225	1	40728
	49973 49973	3	34386	^3E_g	45180	1	40795
	49973	3	34406		45180	1	41733
$^3T_{1g}$		3	36540				
		3	36548				
		3	36602				
^3E_g		5	39661				
		5	39671				
$^3T_{1g}$		3	41659				
		3	41664				
		3	41710				
$^3T_{2g}$		3	41740				
		3	41742				
		3	41852				
^5E_g		3	42923				
		3	42941				
$^1T_{2g}$		1	44395				
		1	44445				
		1	44597				
		1	45531				
		1	45586				
		1	47628				

[a] GCFT calculations in an idealized octahedral (square planar) geometry; *ab initio* CASSCF calculations in the experimental geometry.

Magnetic data

$$\chi = \chi_{para} + \chi_{TIP} + \chi_{dia} + \chi_h + \chi_{PI} \quad \text{(Eq. 1)}$$

The measured magnetic susceptibility consists of the inherent temperature-dependent paramagnetic signal arising from the uncompensated spin and/or orbital angular momentum χ_{para}, temperature-independent paramagnetism χ_{TIP} arising from the close lying excited states, the underlying diamagnetism χ_{dia} and the signal of the sample holder χ_h (usually diamagnetic). Eventually some traces of the dioxygen or other paramagnetic impurities χ_{PI} might be also present so that

On heating, the molar magnetic susceptibility of **1** decreases and passing through the zero it becomes almost constant (Fig. 4). The inherent paramagnetism of a hexacoordinate Co(III) complex possessing the ground electronic term $^1A_{1g}$ is thought to be absent, $\chi_{para} \sim 0$. The low-temperature data refer to the traces of dioxygen that is present in the powder sample and obeys the Curie law. Also, the feature round 50 K is typical for the *solidus-solidus* phase transition of $O_2(s)$.

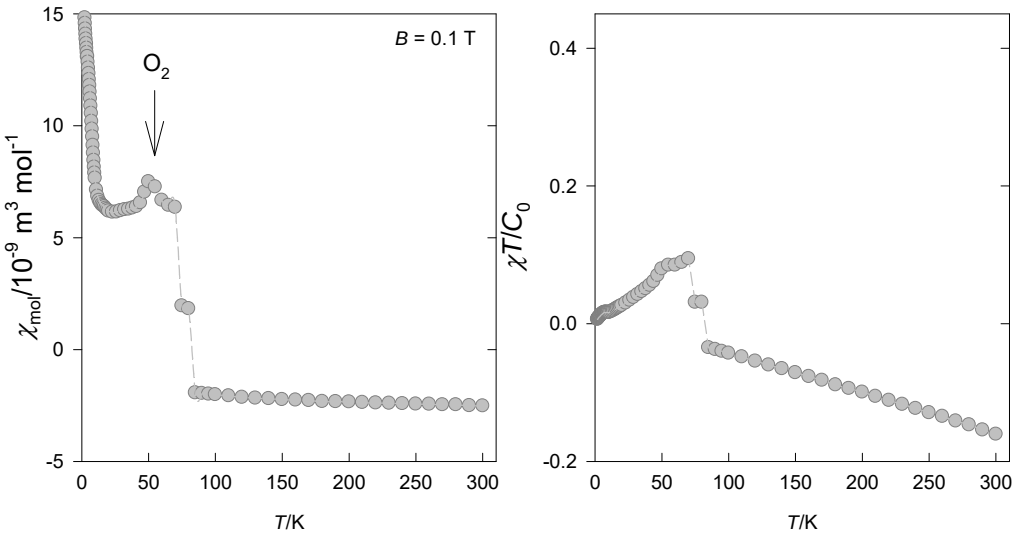

Fig. 4. Magnetic data for **1**. Left – molar magnetic susceptibility (SI units), right – dimensionless product function.

This signal escapes at the room temperature when χ(300 K) = -2.5 × 10^{-9} m^3 mol^{-1} (SI units) consisting only $\chi = \chi_{TIP} + \chi_{dia} + \chi_h$. The underlying diamagnetism can be calculated by means of the Pascal constants, however also a simple estimate using the molar mass M_r can be applied such as χ_{dia} [10^{-12} m^3 mol^{-1}] = -5M_r [g mol^{-1}]; this amounts to χ_{dia} = -2.1 × 10^{-9} m^3 mol^{-1}.

As the excited states of the same multiplicity are far away the ground state the temperature-independent paramagnetic term will be small. It can be hand-calculated by the spin-Hamiltonian formalism that offers the formula

$$\chi_{TIP} = -2N_A\mu_0\mu_B^2(\Lambda_{xx} + \Lambda_{yy} + \Lambda_{zz})/3 \qquad \text{(Eq. 2)}$$

containing the Λ-tensor components (restricted to the first excitation energy)

$$\Lambda_{aa} = -\frac{\left\langle \Psi_0 \left| \hat{L}_a \right| \Psi_1 \right\rangle^2}{E_1 - E_0} \qquad \text{(Eq. 3)}$$

The matrix element of the angular momentum operator for an octahedral Co(III) system is

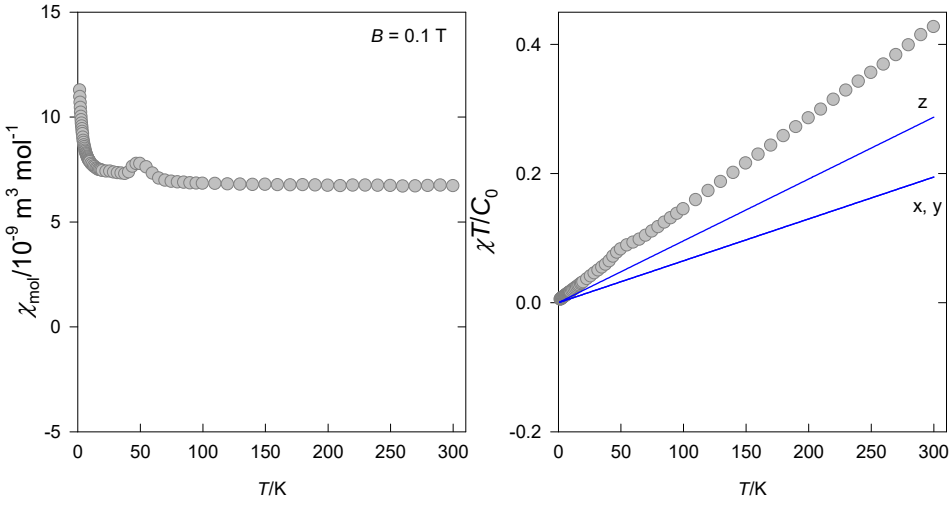

Fig. 5. Magnetic data for **2**. Left – molar magnetic susceptibility (SI units), right – dimensionless product function. Lines – calculated with F_2 = 20 000 and F_4 = 10 000 cm^{-1}.

$\left\langle {}^1\mathrm{A}_1 \left| \hat{L}_{x,y,z} \right| {}^1\mathrm{T}_{1g} \right\rangle = 2$ and using the first singlet excitation energy $\Delta E/hc$ = 21 000 cm^{-1} one gets χ_{TIP} = +2.4 × 10^{-9} m^3 mol^{-1}. The computer evaluation using the generalized crystal field theory yields χ_{TIP} = +3.3 × 10^{-9} m^3 mol^{-1}.

The molar susceptibility for **2** at low temperature starts to decay on heating (Fig. 5), however it reaches almost constant value at the room temperature of χ_{mol} = 6.7 × 10^{-9} m^3 mol^{-1} (SI units). This behaviour clearly deviates from the Curie law. The product function develops according to a straight line and this feature is a fingerprint of a considerable temperature-independent paramagnetism χ_{TIP}. Small anomaly around 50 K is attributed to the *solidus-solidus* phase transition of dioxygen traces which are present in the powder sample. Using the crystal field poles F_2 = 20 000 and F_4 = 10 000 cm^{-1}, the GCFT calculations for a *quadro*-Ni(II) gave χ_{TIP} = +3.1 × 10^{-9} m^3 mol^{-1}.

Conclusions

Two novel low-spin Co(III) and Ni(II) complexes have been prepared and characterized by spectroscopic methods. X-ray structure analysis has shown that the complexes **1** and **2** possess with {CoS6} and {NiS4} chromophore, respectively. The study of bond angles and distances has revealed coordination polyhedron in octahedral (**1**) and square planar (**2**) arrangements. Magnetic studies confirmed a premise on diamagnetic behaviour of both complexes. Our primary goal was to prepare paramagnetic compounds of Co(II) and Ni(II). However, all attempts to prepare such compounds using the *xanth* ligand were unsuccessful.

Acknowledgement

Slovak grant agencies (APVV-14-0078, APVV-16-0039, VEGA 1/0919/17, VEGA 1/0534/16) are acknowledged for the financial support. This article was also created with the support of the MŠVVaŠ of the Slovak Republic within the Research and Development Operation Programme for the project University Science Park of STU Bratislava (ITMS project no. 26240220084) cofounded by the European Regional Development Fund..

References

Boča R, Rajnák C, Titiš J, Valigura D, (2017) Field Supported Slow Magnetic Relaxation in a Mononuclear Cu(II) Complex. Inorg. Chem. 56(3): 1478-1482.

Dolomanov O, Bourhis LJ, Gildea RJ, Howard JAK, Puschmann H, (2009) *OLEX2*: a complete structure solution, refinement and analysis program J. Appl. Crystallogr. 42: 339-341.

Feng X, Mathoniere C, Jeon I, Rouzieres M, Ozarowski A, Aubrey ML, Gonzalez MI, Clerac R, Long JR (2013) Tristability in a light-actuated single-molecule magnet. J. Am. Chem. Soc. 135: 15880-15884.

Frost JM, Harriman KLM, Murugesu M (2016) The rise of 3-d single-ion magnets in molecular magnetism: towards materials from molecules? Chem. Sci. 7: 2470-2491.

Gerloch M, Constable EC (1994) Transition metal chemistry. VCH Publishers, New York, 212 pp.

Grigoropoulos A, Pissas M, Papatolis P, Psycharis V, Kyritsis P, Sanakis Y (2013) Spin-relaxation properties of a high-spin mononuclear Mn(III)O6-containing complex. Inorg. Chem. 52: 12869-12871.

Lin W, Bodenstein T, Mereacre V, Fink K, Eichhofer A (2016) Field-Induced Slow Magnetic Relaxation in the Ni(I) Complexes $[NiCl(PPh_3)_2]\cdot C_4H_8O$ and $[Ni(N(SiMe_3)_2)(PPh_3)_2]$. Inorg. Chem. 55: 2091-2100.

Lomjanský D, Varga F, Rajnák C, Moncoľ J, Boča R, Titiš J (2016) Redetermination of the zero-field splitting in $[Co(qu)_2Br_2]$ and $[Ni(PPh_3)_2Cl_2]$ complexes. Nova Biotechnol. Chim. 15: 200-211.

Lomjanský D, Moncoľ J, Rajnák C, Titiš J, Boča R (2017) Field effect to slow magnetic relaxation in a mononuclear Ni(II) complex. Chem. Commun. 53: 6930-6932.

Mossin S, Tran BL, Adhikari D, Pink M, Heinemann FW, Sutter J, Szilagyi RK, Meyer K, Mindiola JD (2012). A mononuclear Fe(III) single molecule magnet with a 3/2↔5/2 spin crossover. J. Am.Chem. Soc. 134: 13651-13661.

Noro SI, Kitagawa S, Akutagawa T, Nakamura T (2009) Coordination polymers constructed from transition metal ions and organic N-containing heterocyclic ligands: crystal structures and microporous properties. Prog. Polym. Sci. 34: 240-279.

Palatinus L, Chapuis G (2007) SUPERFLIP – a computer program for the solution of crystal structures by charge flipping in arbitrary dimensions. J. Appl. Crystallogr. 40: 786-790.

Rajnák C, Titiš J, Miklovič J, Kostakis GE, Fuhr O, Ruben M, Boča R (2017) Five mononuclear pentacoordinate Co(II) complexes with field-induced slow magnetic relaxation. Polyhedron 126: 174-183.

Rajnák C, Packová A, Titiš J, Miklovič J, Moncoľ J, Boča R (2016) A tetracoordinate Co(II) single molecule magnet based on triphenylphosphine and isothiocyanato group. Polyhedron 110: 85-92.

Saber MR, Dunbar KR (2014) Ligands effects on the magnetic anisotropy of tetrahedral cobalt complexes. Chem. Commun. 50: 12266-12269.

Samuel PP, Mondal KC, Amin Sk N, Roesky HW, Carl E, Neufeld R, Stalke D, Demeshko S, Meyer F, Ungur L, Chibotaru LF, Christian J, Ramachandran V, van Tol J, Dalal NS (2014) Electronic structure and slow magnetic relaxation of low-coordinate cyclic alkyl(amino) carbene stabilized iron(I) complexes. J. Am. Chem. Soc. 136: 11964-11971.

Sheldrick GM (2015) SHELXT – Integrated space-group and crystal-structure determination Acta Crystallogr. A71: 3-8.

Sheldrick GM (2015) Crystal structure refinement with *SHELXL*. Acta Crystallogr. C71: 3-8.

Yang F, Zhou Q, Zhang Y, Zeng G, Li G, Shi Z, Wang B, Feng S (2013) Inspiration from old molecules: field-induced slow magnetic relaxation in three air-stable tetrahedral cobalt(II) compounds. Chem. Commun. 49: 5289-5291.

Zadrozny JM, Long JR (2011) Slow magnetic relaxation at zero field in the tetrahedral complex $[Co(SPh)_4]^{2-}$. J. Am. Chem. Soc. 133: 20732-20734.

Zadrozny JM, Telser J, Long JR (2013) Slow magnetic relaxation in the tetrahedral cobalt(II) complexes $[Co(EPh)_4]^{2-}$ (E = O, S, Se). Polyhedron 64: 209-217.